CHAPTER IV
IRON LOADED MCM-41 VIA SOL-GEL TECHNIQUE AND ITS ACTIVITY

4.1 Abstract

MCM-41, one of the most important members of the M41S family, has attracted the attention of scientists due to its outstanding characteristics. To provide solids with potential catalytic applications, it is possible to modify the nature of the framework by incorporating heteroelements into MCM-41 structure, and iron is known to be an active center of catalysts for several oxidation reactions. Thus, in this work, iron-containing mesoporous molecular sieve or Fe-MCM-41 was synthesized via sol-gel technique and characterized using XRD, DRUV, ESR, XRF and BET methods. Many factors were investigated, such as, reaction temperature, time, calcinations rate and metal amount in the reaction mixture, and it was found that the optimum condition to synthesize Fe-MCM-41 by using silatrane and $FeCl_3$ as the silicon and iron sources, respectively, was to carry out the reaction at 60°C for 7 hrs and the calcinations rate of 1°C/min at 550°C calcinations temperature. The catalytic activity and selectivity of styrene epoxidation using hydrogen peroxide were studied, and showed that the selectivity of styrene oxide reached 65% at styrene conversion of 22% over the 1%wt catalyst.

Keywords: Fe-MCM-41, Silatrane, Sol-gel process and Styrene epoxidation

4.2 Introduction

In late 80s, Mobil's researchers successfully synthesized a new family of mesoporous silicate and aluminosilicate molecular sieves, designated as M41S, including MCM-41 (hexagonal), MCM-48 (cubic) and MCM-50 (laminar) synthesized with liquid crystal templates possessing a well-order array of structure and a uniform pore size distribution in the range from 15 to 100 Å. MCM-41, possessing a hexagonal arrangement of channels, is one of the most important member of the M41S family [15], and has attracted the attention of scientists due to its elevated specific surface area, high thermal and hydrothermal stability, possibility of controlling its pore size, its hydrophobicity and acidity. These characteristics have made MCM-41 a promising material as catalyst and/or catalyst support to be used in industrial processes of adsorption, ion exchange and environmental control, hosts for the inclusion of compounds and nanosize clusters, and molecular sieves for large molecules [13].

There are 2 types of surfactants, supramolecular templating and liquid-crystal templating (LCT). Many research groups exploited this technique of supramolecular templating to produce not only mesoporous silicate and aluminosilicate materials, but also mesostructured metal oxides. The extension of this liquid-crystal templating (LCT) mechanism into the field of transition metal oxide synthesis represented a major step forward towards tailoring catalytic, electronic and magnetic properties of these redox-active materials [14].

However, only pure silica MCM-41 limits their catalytic applications. It is known that incorporation of transition-metal ions in the silica framework may improve the catalytic performance of MCM-41. Many researchers have tried to introduce other compound into the silica-based MCM-41 framework and iron, one of the significant transition metals, was celebrated [1]. Fe-containing MS or molecular sieve can be prepared using iron salts, such as, iron nitrate [$Fe(NO_3)_3 \cdot 9H_2O$] as iron source. Modification of MMS or mesoporous molecular sieve (MCM-41, MCM-48 or HMS) by incorporation of transitional ions, Fe^{3+} ion, for example, is well documented. There are two ways in which the iron can modify the silica structure. The iron may well be incorporated by substitution into the silica framework in a tetragonal

geometry, and thus be attached by *covalent* bonds. In the other way, the metal may simply be in contact with the surface of the pore walls, and upon calcinations, nanoclusters of octagonal crystalline iron oxide (Fe_2O_3), so called "*extra-framework*", are formed. This *extra-framework* iron is retained to the support only by *weak* Van der Waals bonds. The major problem with iron atoms is the formation of extra-framework iron species during template removal by calcinations [10]. Synthesis of Fe-MMS with maximum incorporation of Fe (Si/Fe ratio of about 10) was performed in neutral conditions using primary amines. These Fe-MMS were also found to be very active and selective catalysts (100%) for the benzylation of benzene, oxidation (hydroxylation of aromatic compounds and epoxidation of olefins), polymerization and oligomerization of propene [6].

In the recent years, metal ion-incorporated MCM-41 has attracted much attention as oxidation catalyst. For example, Ti-MCM-41 was reported to catalyze various oxidation reactions with H_2O_2, but the epoxidation of cyclohexene could not proceed selectively over the catalyst with diluted H_2O_2, or Mn-MCM-41 showed high selectivity for the epoxidation of stilbene with *tert*-butyl peroxide or TBHP [6]. Recently, an iron-immobilized MCM-41 modified with organic silane exhibited activity in the oxidation of cyclohexane to cyclohexanol and cyclohexanone at 373 K with H_2O_2 [4], The highest conversion of styrene over the Fe-MCM-41 via direct hydrothermal technique showed 14% conversion over 1.1 wt% Fe catalyst [17]. Moreover, the activity and efficiency of H_2O_2 increases with the metal content and reaction parameters, such as temperature [2].

In this work, MCM-41 and Fe-MCM-41 were synthesized using moisture stable silatrane and $FeCl_3$ as the precursors. The synthetic conditions were studied to obtain the optimal condition for high surface areas of both products. More importantly, their oxidation activities on styrene were investigated, as well.

4.3 Experimental

4.3.1 Materials

Fumed silica (SiO_2) from Aldrich Chemical Co., UHP grade nitrogen (N_2, 99.99% purity) from Thai Industrial Gases Public Company Limited (TIG), ethylene

glycol (EG), triethanolamine (TEA) and acetonitrile (CH_3CN) from Labscan were used for silatrane synthesis. Ferric Chloride ($FeCl_3$) from Aldrich Chemical Co., hexadecyltrimethyl amonium bromide (CTAB) from Sigma Chemical Co. and sodium hydroxide (NaOH) from Univar were used for Fe-MCM-41 synthesis. Styrene monomer and dimethylformamide (DMF) from Labscan, hydrogen peroxide from Carlo Erba were used for activity study.

4.3.2 Synthesis

Following the method of Wongkasemjit, silatrane, as silicon source, was synthesized directly from inexpensive and widely available starting materials, SiO_2 and TEA, via the Oxide One Pot Synthesis (OOPS) process [11]. Fe-MCM-41 was synthesized via the one-step synthesis using silatrane and $FeCl_3.6H_2O$ as silicon and iron sources, respectively. The composition of the reactants is followed the previous study on the synthesis of extremely high surface area MCM-41 [16]. The formula used was *x*silatrane: *y*$FeCl_3.6H_2O$:*0.014*TEA:*0.5*CTAB:*0.001*NaOH:*0.36*H_2O. To study the optimal condition for Fe-MCM-41 synthesis, iron concentration, synthesis time, reaction temperature, calcinations rate as well as metal amount were varied.

4.3.3 Characterization

FTIR spectroscopic analysis was conducted on a Bruker Instrument (EQUINOX55) with a scanning resolution of 4 cm^{-1}. Thermal properties were analyzed by thermogravimetric analysis (TGA) on Du Pont Instrument TGA 2950 with the N_2 flow rate of 50 ml per min. Mesoporous product was characterized using a Rigaku X-ray diffractometer at a scanning speed of 2°/sec and CuKα as source. Diffuse reflectance UV-vis (DR-UV) spectra were recorded on a SHIMADZU UV-2550 UV-VISIBLE spectrophotometer. Powdery sample was loaded in a teflon cell, and the spectra were collected in 190-600 nm range with a reference of $BaSO_4$. Surface area and average pore size were measured by BET method using a Quantasorb JR. (Autosorb-1). The product was degassed at 250°C for 10 hrs before analysis. ESR spectra were measured at X-band, ~9 GHz, on a ESPRIT-425 vol.604 spectrometer. The sample was placed in a quartz tube with an inner 3 mm in diameter and measured at ambient temperature. X-ray fluorescence spectroscopy or XRF

(Bruker Model SRS 3004) was used to determine the amount of Fe waiting for the specification.

4.3.4 Catalytic Reaction

The epoxidation of alkene (styrene) was carried out using a batch-type reactor. Catalyst (x g.), styrene (10 mmol), H_2O_2 (10 mmol, 30 wt% aqueous solution) and DMF (10 mL) were added in a glass flask. The reactant mixture was stirred vigorously. The factors studied were amount of catalyst, temperature, time, and amount of iron loaded. Generally, styrene oxide and benzaldehyde were two main products in the epoxidation of styrene with H_2O_2 over Fe–MCM-41 [17]. However, styrene glycol and benzoic acid were also formed with low selectivity [17]. All liquid products were quantified using a gas chromatograph with a capillary column (DB-WAX, 30 M×0.25 mm) and a FID detector. The consumption of H_2O_2 was determined by iodometric titration.

4.4 Results and Discussions

4.4.1 Characterization of Silatrane Precursor

Since the synthesis was followed the previous work [11], a few characterization was performed to confirm the right product. FTIR spectrum as seen in figure 4.1 shows the characteristic peaks of silatrane at 785 to 729 and 579 cm^{-1} corresponding to Si-O-C and Si<---N, respectively. Moreover, TGA result in figure 4.2 shows one sharp mass loss transition at 400°C with 18.5 %ceramic yield corresponding to $Si((OCH_2CH_2)_3N)_2H_2$.

4.4.2 Characterization of Fe-MCM-41 Catalyst

Fe-MCM-41 was synthesized by using CTAB as a template. Via liquid crystal templating mechanism (LCT), the pore will mimic the surfactant liquid crystal structure. General procedure for synthesizing Fe-MCM-41 using SiO_2 precursor, needs to use high temperature and long reaction time in autoclave [16]. Thus, commercially available alkoxide precursor, such as, tetraethoxysilane (TEOS), tetramethoxysilane (TMOS) or sodium silicate, is often used to reduce reaction temperature and time. However, these precursors are expensive compared with SiO_2. Recently, Fe-MCM-41 was synthesized from sodium silicate precursor via direct

hydrothermal and template ion exchange method. The product via direct hydrothermal method gave a good quality of Fe-MCM-41 with surface area of 1100 m^2g^{-1} at 1% iron loaded, but it took more than 2 days for aging the sample, and more extra-framework occurred [17]. Recently, Wongkasemjit's method using silatrane precursor synthesized from an inexpensively starting material SiO_2 successfully provided extremely high surface area MCM-41 [16]. Following this method, high quality of Fe-MCM-41 having remarkable surface area up to ~1800 m^2/g at 1% iron loaded was satisfyingly synthesized at lower reaction temperature and shorter aging time.

Generally, the XRD pattern of MCM-41 showed the diffraction lines of (100), (110) and (200) at 2θ/θ of ca. 2.2, 3.6, and 4.3, respectively, indexing to the hexagonal regularity of MCM-41. Those three characteristic lines were also observed in this case of Fe–MCM-41 samples. Moreover, DR-UV used to determine the site of iron and also the presence of Fe extra-framework showed that all samples exhibited a peak at ca. 240-300 nm similar to ferrisilicate containing tetrahedrally coordinated iron species [17]. This band is assigned to the $d\pi$–$p\pi$ charge transfer between the Fe and O atoms in the framework of Fe–O–Si in the zeolite. The contribution at long wavelength to this band became larger with an increase of Fe content. Moreover, the presence of extra-framework iron or aggregated Fe oxide clusters at high Fe content showing the bands at ca. 385 and 510 nm, which were mainly observed for Fe_2O_3, suggests that there is an upper limit of iron content incorporated inside the framework of MCM-41 [17].

4.4.2.1 Effect of Temperature

It is known that temperature affects to the liquid crystal formation. When increasing the mixing temperature from 40° to 100°C at 1% Fe loaded for 3 hrs [16], XRD spectra showed a sharper peak with a little shift of peaks to the lower degree two theta, as shown in figure 4.3, referring to bigger pore sizes. The reason may come from the fact that the higher temperature makes the surfactant tail more flexible to move or vibrate more freely, causing more occupied space of surfactant in the pore, as a result, causing a bigger pore after removing the surfactant. The diameters at 40° and 100°C are 21 and 32 Å, respectively. This size is close to that of CTAB micelle, ~39 Å. [16]. Coincidently, Cheng used the sorption technique as our work

showed the increase in channel diameter from 27.1 to 36.5 Å when increasing temperature from 70° to 165°C for the reaction time of 48 hrs [5]. However, in this work when increasing temperature up to 60°C, the XRD spectrum showed clearly pattern of MCM-41, giving distinguishable peaks of the 110 and 200 reflections, caused from the long range order of hexagonal array. As a result, surface area and pore volume of Fe-MCM-41 obtained from using silatrane are impressively high and much higher than atrane synthesized from another route [2,17], probably due to a purer silatrane product obtained, as shown in table 4.1. In addition, DR-UV results in figure 4.4 show the peak of the framework around 260-300 nm, indicating Fe incorporation in the MCM-41 framework, without the peak of extra-framework. At lower 60°C, less iron can be incorporated inside the framework due to the smaller pore size, making more difficult for iron atom to be incorporated. At too high temperature, ~100 °C, less amount of iron can be incorporated due to the degradation of TEA, thus, the hydrolysis and condensation reaction are chaotic [18]. The results can be confirmed by using XRF to determine the amount of iron, as shown in the table 4.2.

4.4.2.2 Effect of Aging Time

In this study, aging time representing the time between the formation of gel and the removal of solvent is another important factor. For alkoxide-derived gel, condensation between surface functional groups continues to occur after gel point. During aging, there are changes in most texture and physical properties of the gel. The strength of the gel thereby increases with aging. When increasing the aging time from 3 to 13 hr at 1% Fe loaded at the mixing temperature of 60°C, XRD spectra do not significantly showed any difference, as indicated in previous work [16]. The 110 and 200 reflections were not obviuosly separated, as shown in figure 4.5, when the aging time reached 13 hrs, meaning that the hexagonal array can not be formed perfectly [16]. DRUV results show most amount of iron incorporated inside the framework at 7 hr aging time (figure 4.6). The shorter aging time, less than 7 hrs, the less iron incorporated inside the framework due to not enough time for the reaction to occur. At longer aging time than 7 hrs, less amount of iron was also incorporated due to the degradation of TEA and the reverse condensation reaction [18]. The

results are confirmed by XRF providing the amount of iron in the sample, as listed in table 4.3. BET surface area, pore size and pore volume are summarized in table 4.4. It was found that the aging time also gave no effect on the surface area or pore volume, as coincided with the XRD results.

4.4.2.3 Effect of Calcinations Rate

The major problem with iron atoms is the formation of extraframework iron species during template removal by calcinations. Some works reported that iron oxide clusters colored the materials in shade of brown, whereas framework iron is colorless [10]. Iron can be incorporated in the silica framework through direct synthesis by introducing an appropriate iron precursor in the synthesis gel, as done for other atoms, such as, titanium or boron. Using this way, iron atoms present at the edge of the pore walls are likely to represent resistantly active centers [10]. Substitution is more difficult than simple contact to the surface and there is often a mixture of both framework and extra-framework metal species when substitution was intended [17]. Thus, calcinations rate was studied to find the condition for the least extra-framework, and the structure and surface area were well existed.

Calcinations rate was varied from 0.5 to 11°C/min at 1 % Fe loaded and the mixing temperature of 60°C for 7 hr. XRD patterns showed lower crystallinity when increasing the calcinations rate, as shown in figure 4.7. DRUV spectra in figure 4.8 show the extra-framework observed at the wave number of 360 nm and even more obvious when increasing the calcinations rate more than 3°C/min. The results are also confirmed using ESR technique in figure 4.9. There were two signals at g = 2.0 and 4.3. It was reported that the signal at g = 4.3 could be attributed to Fe(III) in tetrahedral coordination with strong rhombic distortion or framework form, and at g = 2.0 in octahedral coordination or extraframework form [3,7]. When increasing the calcinations rate, the signal at g = 2.0 became strong and broad. It could be considered that the octahedral coordinated iron exists more in the structure. However, the calcinations rate did not significantly change surface area, as shown in table 4.5.

4.4.2.4 Effect of Amount of Fe Loaded

The calcined products at 0.5-2.5 %Fe loaded showed a well-resolved pattern of the hexagonal mesostructure, see figure 4.10. However, at high %Fe loaded, the

XRD patterns showed lower crystalline phase, as indicated at the 100 reflection peak, and less isolation of 110 and 200 reflections peaks. The DRUV spectra in figure 4.11 show the extra-framework observed at the wave number of 380 nm when the %Fe loading increased and more obvious when the %Fe loaded higher than 2.1%. The results can be confirmed using ESR technique (figure 4.12) When increasing the amount of Fe, the signal at g = 2.0 turned strong and observable XRF in table 4.6 show the amount of iron in the samples which are closely to the actual loading. It was found that most of the iron loaded exists in the sample at different positions, framework and extra-framework forms. Thus, when increasing the amount of iron loaded, the color of the sample was changed from white to brown, see table 4.6. For BET results in table 4.7, the surface area was decreased but the pore size and pore volume were increased due to the larger ionic radius of Fe^{3+} than that of Si^{4+} [17].

4.4.3 Catalytic Activity in Styrene Epoxidation Reaction

The following factors were studied to find the best activity of our synthesized Fe-MCM-41;

4.4.3.1 Reaction Temperature

The reaction formula in this work was following Wang's study [17], and it was found that (table 4.8 and figure 4.13) styrene conversion reached 22 % at 60°C. According to Zhang's study [12], styrene oxide and benzaldehyde were two main products in the epoxidation of styrene with H_2O_2 over Fe–MCM-41 while styrene glycol and benzoic acid were also formed with low selectivity [12]. In our case, the activity resulted in only styrene oxide and benzaldehyde at 64.86 and 35.14%, respectively, without styrene glycol and benzoic. However, styrene glycol and benzoic acid occurred observably when increasing the reaction temperature.

4.4.3.2 Reaction Time

Using the same reaction formula, styrene conversion went up sharply at initial stage, and reached a steady state at ~ 22% after 1 hr reaction time, as shown in figure 4.13. H_2O_2 was also decomposed very quickly at the initial stage and its conversion reached ~90% after 1 hr of reaction. When increasing the reaction time the conversion of styrene did not change unambiguously (figure 4.13) , and additionally benzoic acid occurred observably, as shown in figure 4.14

4.4.3.3 Amount of Catalyst

Figure 4.15 shows that at 0.1 g of catalyst styrene conversion reached 22% and %conversions of styrene oxide and benzaldehyde were 64.68 and 35.31, respectively, without the presence of styrene glycol and benzoic acid. Moreover, styrene conversion did not change significantly when compared with 0.2 g and 0.3 g of catalys, in which the reaction time reached a steady state faster than 0.1%, as shown in figure 4.15, but it was not significantly different in efficiency of the catalyst.

4.4.3.4 Amount of Fe Loaded

From the previous factor, the optimal condition for styrene epoxidation over synthesized Fe-MCM-41 is at 0.1 g of catalyst and 60°C reaction temperature for 2 hr. The next factor studied was the amount of Fe loaded. Figure 16 shows the results of epoxidation of styrene with diluted H_2O_2. Conversion of styrene was very low over pure MCM-41, although, the conversion of H_2O_2 reached 50 %, suggesting that iron was mainly responsible for the conversion of styrene with H_2O_2. The increase in Fe content up to 1 % increased the conversion of styrene observably and the selectivities of styrene oxide and benzaldehyde were 64.68 and 35.31%, respectively, without any styrene glycol and benzoic acid. When Fe content was up more than 1%, the conversion of styrene was rather slightly decreased although the conversion of H_2O_2 still went up. Moreover, styrene glycol and benzoic acid were also observed. In addition, Fe impregnated MCM-41 used as a catalyst was also studied to compare with the catalyst synthesized the via sol-gel technique. It was found that conversion of H_2O_2 was very high, but the conversion of styrene and the selectivity of the products were very low. The results shown in table 4.9 combined with the characterization results described above suggest that the iron sites incorporated inside the framework of MCM-41 probably account for the epoxidation of styrene with H_2O_2, whereas the iron oxide clusters or iron species in the extraframework position seem to accelerate the decomposition of H_2O_2.[17]

4.5 Conclusions

Silatrane synthesized via the OOPS process is an excellent precursor for the synthesis of Fe-MCM-41. The optimal condition maintaining the hexagonal array of MCM-41 structure is at 60°C reaction temperature for 7 hrs, 550°C calcinations temperature and 1°C/min calcinations rate. When increasing the amount of Fe loading, the XRD patterns showed lower crystalline material. However, the obtained Fe-MCM-41 keeps the structure of MCM-41 even using 2.5% Fe loaded. The extraframework is observed when the %Fe loading is more than 2.1%. The iron cations could exist either outside the framework or inside the framework of MCM-41, but the irons inside the framework were responsible for the conversion of styrene with H_2O_2 aqueous solution. The selectivity of styrene oxide reached 65% at styrene conversion of 22% over the 1% loaded Fe. Moreover, when compared with the impregnated catalyst, the sol-gel synthesis catalyst shows a much better performance for the epoxidation of styrene.

4.6 Acknowledgements

This research work is supported by the Postgraduate Education and Research Program in Petroleum and Petrochemical Technology (ADB) Fund, Ratchadapisake Sompote Fund, Chulalongkorn University and The Thailand Research Fund (TRF).

4.7 References

1. A. Tuel, S. Gontier, R. Teissier (1996). Chem. Commun. 32, 651-660.
2. B.-L. Su, V. Parvulescu (2001), Catalysis Today, 69, 315-322
3. Bordiga, S, Buzzoni, R., Geobaldo, F., Lamberti, C., Giamello, E.,Zecchina, A., Leofanti, G., Petrini, G., Tozzola, G., and Vlaic, G. (1996), J. Catal. 158, 486.
4. Carvalho A.,Wallau M., and Schuchardt U. (1999), J. of Molec. Catal. A, 144, 91-99.

5. Cheng F. C., Zhou W., Klinowski J., (1996), Chem. Phys. Lett. 263, 247-252.
6. D. Trong On, D. Desplantier-Giscard1, C. Danumah, S. Kaliaguine (2003), Applied Catalysis A:General 253, 545–602.
7. Derouane, E. G., Mestsdagh, M., and Vielvoye, L. (1974), J. Catal. 33, 169.
8. IUPAC Manual of Symbols and Terminology for Physiochemical Quantities and Units (1972): Appendix II. Butterworths, London, 31, 578-638.
9. N. Phonthammachai , T. Chairassameewong, E. Gulari, A.M. Jamison, S. Wongkasemjit (2003). Microp and Mesop Mat. 66, 261-271.
10. Nicolas Crowther, Faïçal Larachi (2003), Applied Catalysis B: Environmental 46, 293–305.
11. Piboonchaisit, P., Wongkasemjit, S. and Laine, R. (1999), Science-Asia, J.Sci. Soc. Thailand, 25, 113-119.
12. Qinghong Zhang, Ye Wang, Satoko Itsuki, Tetsuya Shishido, and Katsuomi Takehira (2001), Chemistry Letters, CL-010566, 946-947
13. Ryong Ryoo, Shinae Jun (1997), J. Phys.Chem. B , 101, 317-320.
14. S. Sadthayanon. The Petroleum and Petrochemical Callage, Chulalongkorn University, 2003.
15. S.H. Liu, H. Paul Wang (2002). International Journal of Hydrogen Energy. 27, 859-862.
16. Thanabodeekij, N., The Petroleum and Petrochemical College, Chulalongkorn University, 2003.
17. Ye Wang, Qinghong Zhang, Tetsuya Shishido, and Katsuomi Takehira (2002), J. of Catal, 209, 186–196.
18. Yilmaz, V.T., Topcu, Y. and Karadag, A. (2002), Thermchimica Acta, 383, 129-133.

Table 4.1 The BET analysis of Fe-MCM-41 synthesized at different temperatures

Temperature (°C)	BET Surface Area (m^2/g)	Pore Volume (cc/g)	Average Pore Size (Å)
40	1314	1.060	21
60	1625	1.208	22
80	1553	1.403	30
100	1290	1.090	32

Table 4.2 The XRF analysis of Fe-MCM-41 synthesized at different temperatures

Temperature (°C)	Fe content in sample by XRF (%)	Color of sample	
		As synthesized	Calcined
40	0.893	White	Off white
60	0.991	White	Off white
80	0.943	White	Off white
100	0.804	White	Off white

Table 4.3 The XRF anaiysis of Fe-MCM-41 synthesized at different aging times

Aging time (hours)	Fe content in sample by XRF (%)	Color of sample	
		As synthesized	Calcined
3	0.87	White	Off white
5	0.937	White	Off white
7	1.078	White	Off white
9	0.993	White	Off white
11	0.956	White	Off white
13	0.945	White	Yellow

Table 4.4 The BET analysis of Fe-MCM-41 synthesized at different aging times

Time (hrs)	BET Surface Area (m^2/g)	Pore Volume (cc/g)	Average Pore Size (Å)
3	1504	1.12	26
5	1568	1.09	26
7	1698	1.12	27
9	1407	1.12	27
11	1395	1.14	28
13	1309	1.08	27

Table 4.5 The BET analysis of Fe-MCM-41 synthesized at different calcinations rates

Calcination Rate (^{0}C/min)	BET Surface Area (m^2/g)	Pore Volume (cc/g)	Average Pore Size (Å)
0.5	1798	1.11	26
1	1783	1.15	27
3	1759	1.13	26
5	1755	1.17	27
7	1734	1.18	26
9	1725	1.12	26

Table 4.6 The XRF analysis of Fe-MCM-41 synthesized at different calcinations rates

% Loaded Fe	Fe content in sample by XRF (%)	Color of sample	
		As synthesized	Calcined
0	0	White	White
0.5	0.544	White	White
1	1.078	White	White
1.3	1.332	White	Off white
1.5	1.495	White	Off white
2.0	2.005	White	Off white
2.1	2.088	White	Off white
2.2	2.195	White	Yellow
2.5	2.465	White	Yellow

Table 4.7 The BET analysis of Fe-MCM-41 synthesized at different amount of loaded Fe

Loaded Fe (%)	BET Surface Area (m^2/g)	Pore Volume (cc/g)	Average Pore Size (Å)
0	1885	1.16	24
0.5	1823	1.16	25
0.8	1787	1.18	27
1	1724	1.20	28
1.3	1588	1.21	28
1.5	1539	1.21	30
1.8	1227	1.23	31
2.0	1208	1.24	32
2.3	1052	1.28	32
2.5	989	1.31	34

Table 4.8 Effect of temperature for epoxidation of styrene at 2 hr

Temp (°C)	Sty conv (%)	H_2O_2 conv (%)	Selectivity (%)				H_2O_2 eff(%)
			Sty oxi	Benzald	Sty gly	Benz â	
40	15	85	49.1	50.9	-	-	8.84
50	17.99	91	55.43	44.57	-	-	11.31
60	22	93	64.89	35.14	-	-	15.67
70	21.32	96	42.87	44.25	4.56	8.32	9.71

Note!

$$H_2O_2 \text{ efficiency (\%)} = \frac{\text{Amount of styrene oxide formed (mol)}}{\text{Amount of } H_2O_2 \text{ consumed (mol)}} \times 100$$

Table 4.9 Comparison of catalysts for epoxidation of styrene

Catal (%)	Sty conv (%)	H_2O_2 conv (%)	Selectivity (%)				H_2O_2 eff(%)
			Sty oxi	Benzald	Sty gly	Benz â	
0% Fe (s – g)	3.32	49	36.77	53.75	-	-	2.54
1% Fe (s – g)	21.89	91	64.68	35.31	-	-	15.88
2% Fe (s – g)	19.12	98	62.79	29.33	3.56	4.32	12.5
1% Fe (imp)	9.23	100	41.05	44.76	3.21	10.98	3.87
2% Fe (imp)	11.26	100	43.06	32.84	5.67	18.43	4.95

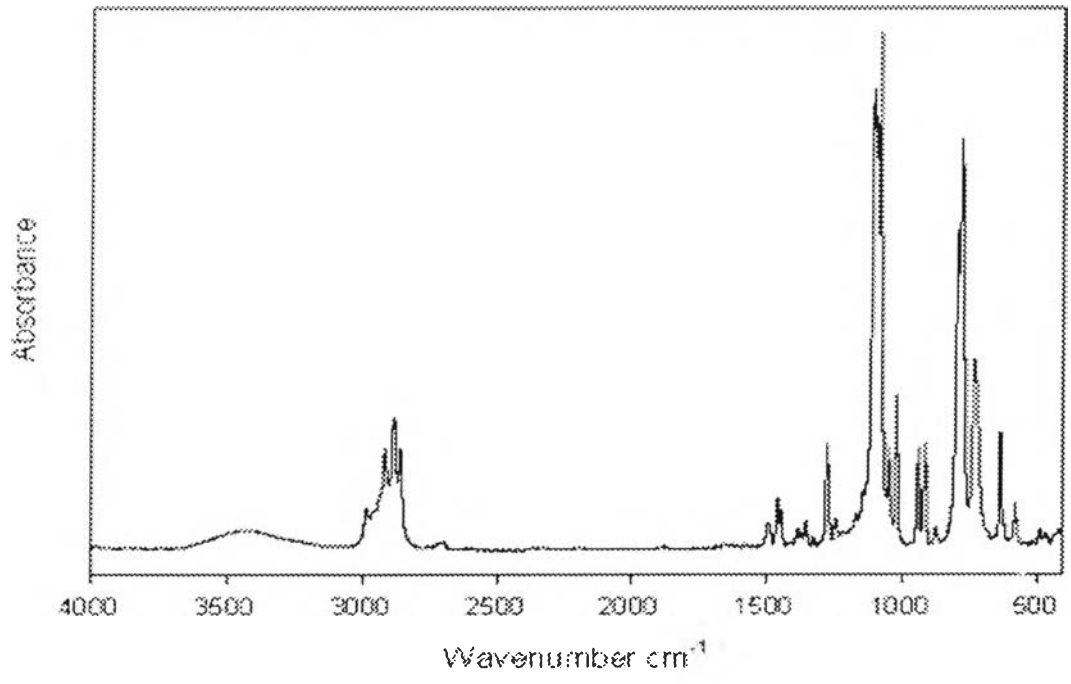

Figure 4.1 FTIR spectrum of silatrane precursor.

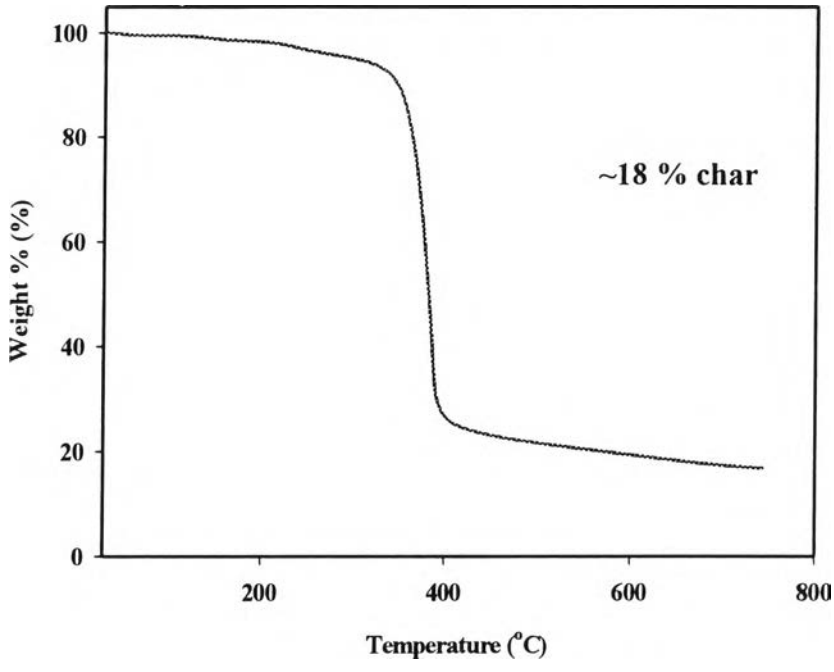

Figure 4.2 TGA result of silatrane precursor.

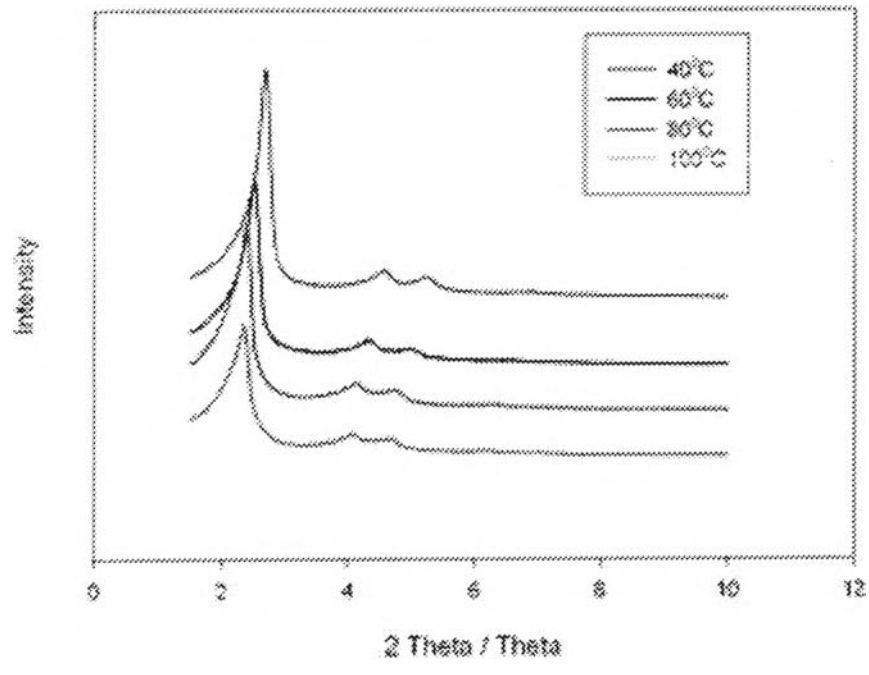

Figure 4.3 The XRD spectrum of synthesized MCM-41 at different temperatures.

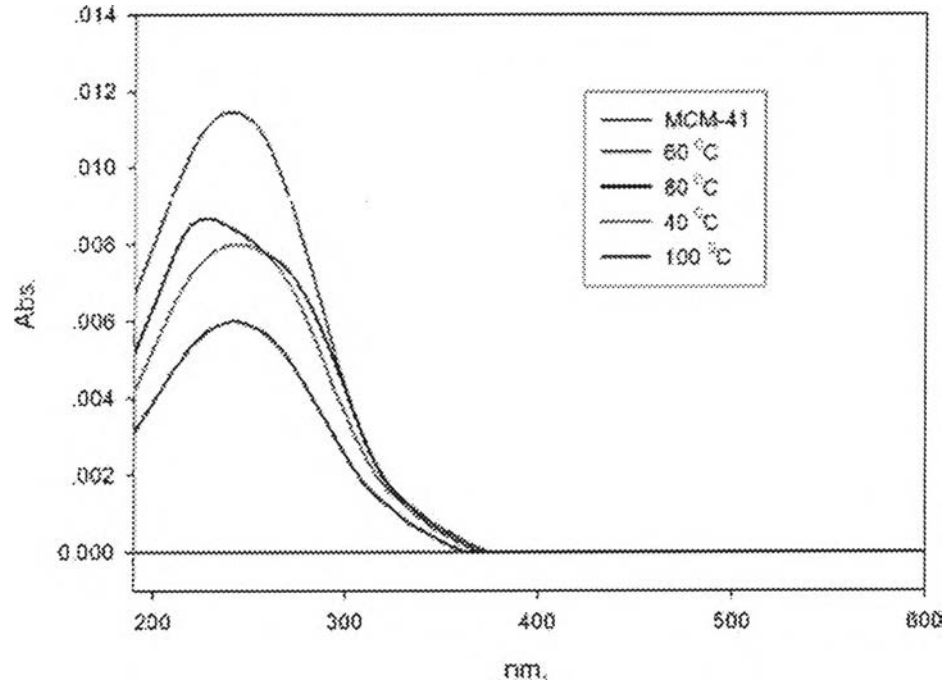

Figure 4.4 The DR-UV sprctra of synthesized Fe-MCM-41 at different temperatures.

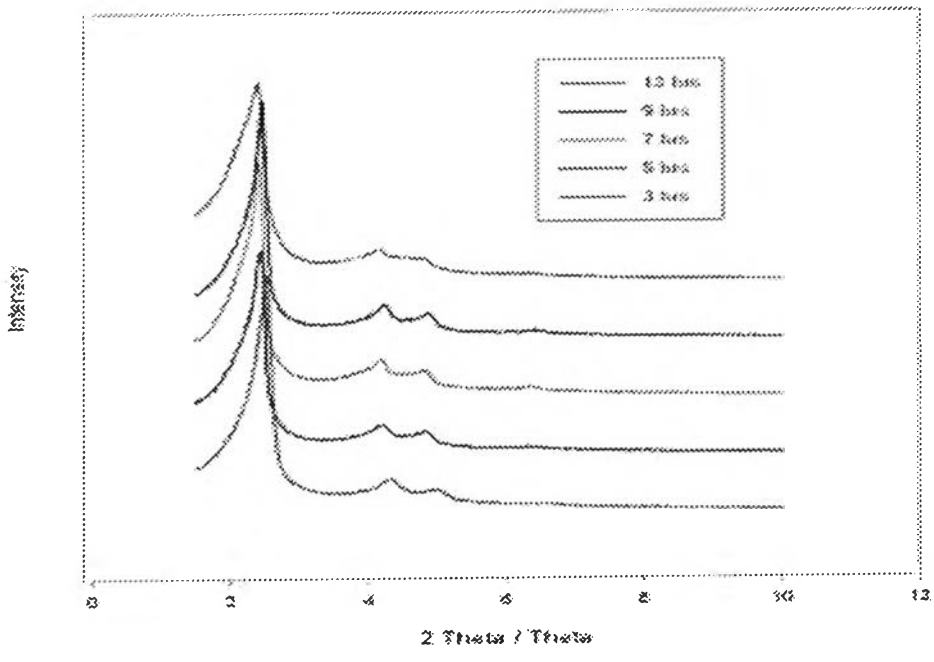

Figure 4.5 The XRD spectrum of synthesized MCM-41 at different aging times.

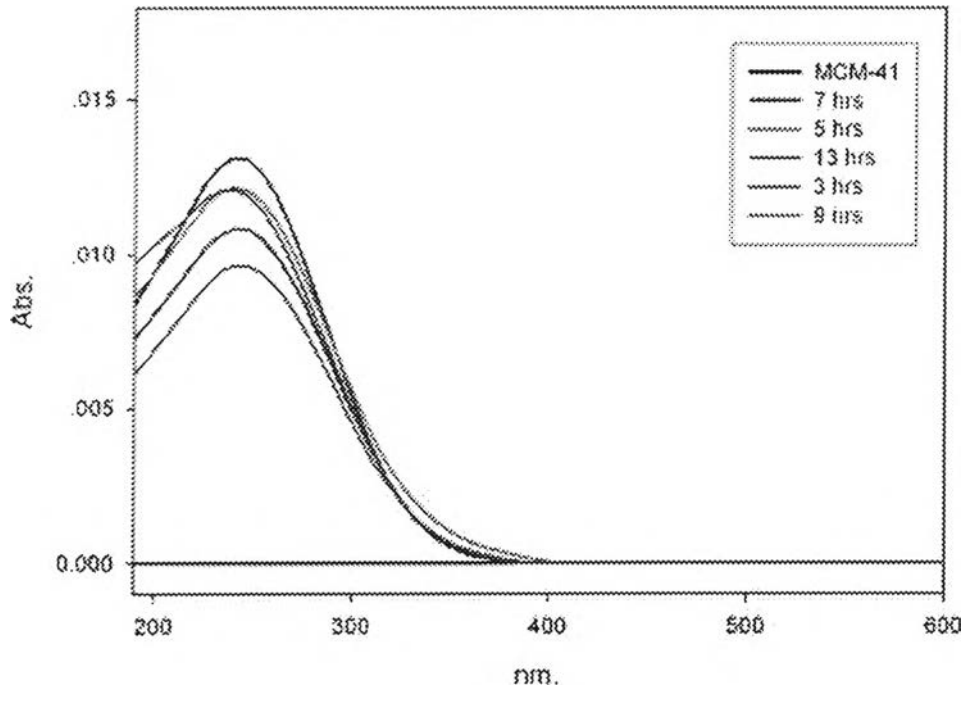

Figure 4.6 The DR-UV sprctra of synthesized Fe-MCM-41 at different aging times.

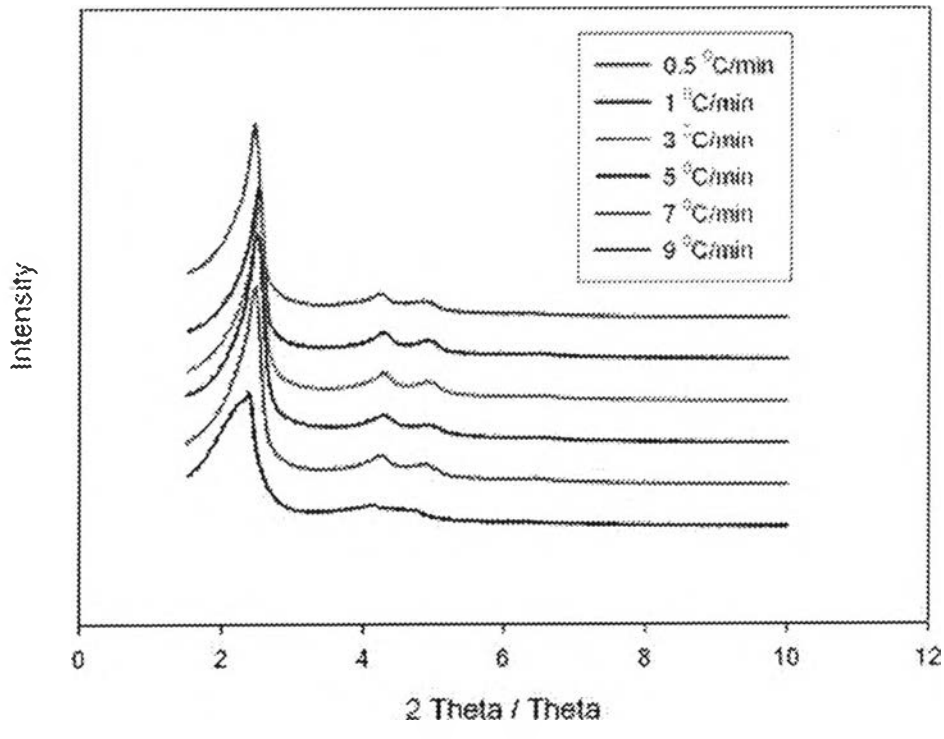

Figure 4.7 The XRD spectrum of synthesized MCM-41 at different calcinations rates.

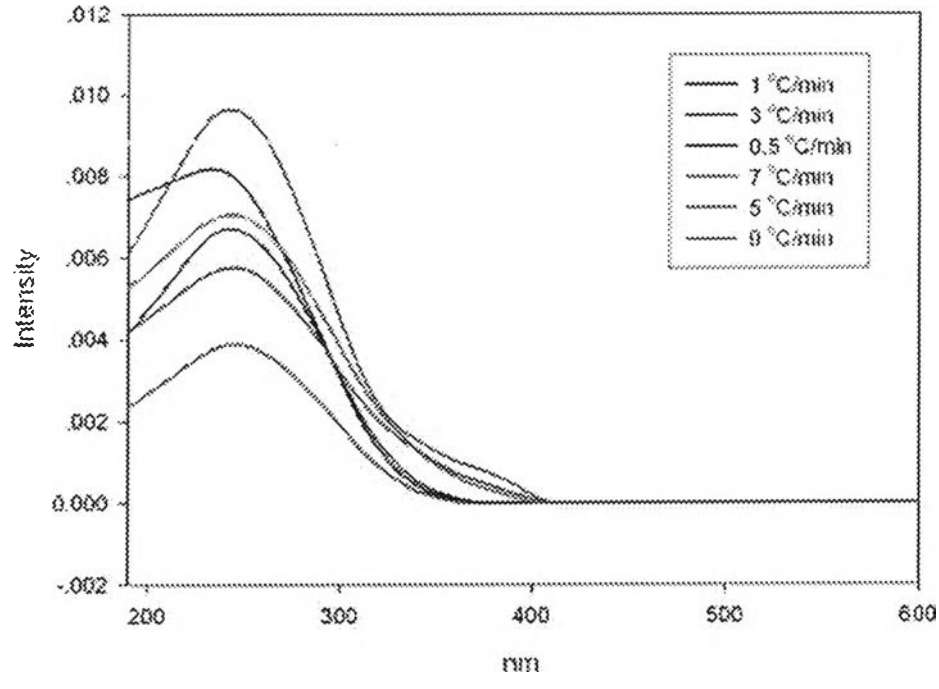

Figure 4.8 The DR-UV sprctra of synthesized Fe-MCM-41 at different calcinations rates.

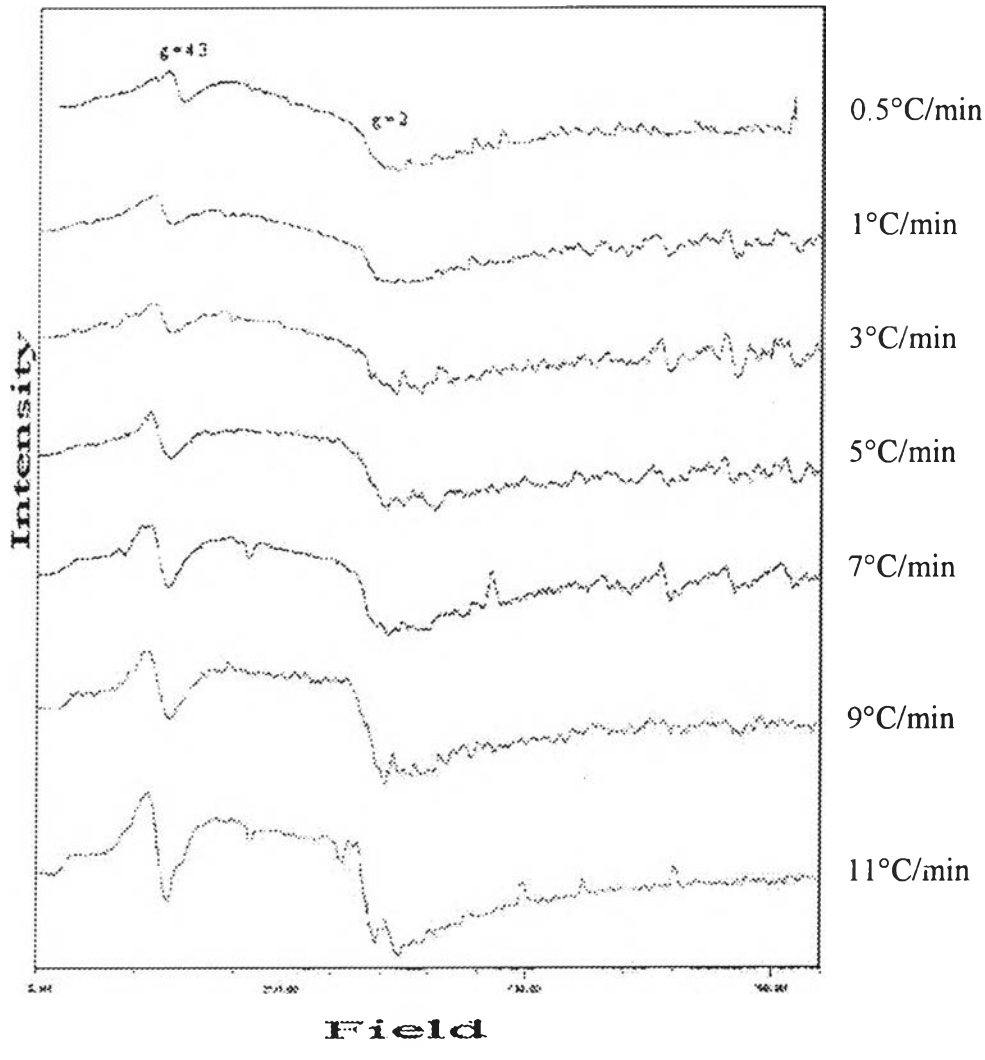

Figure 4.9 The ESR sprctra of synthesized Fe-MCM-41 at different calcinations rates.

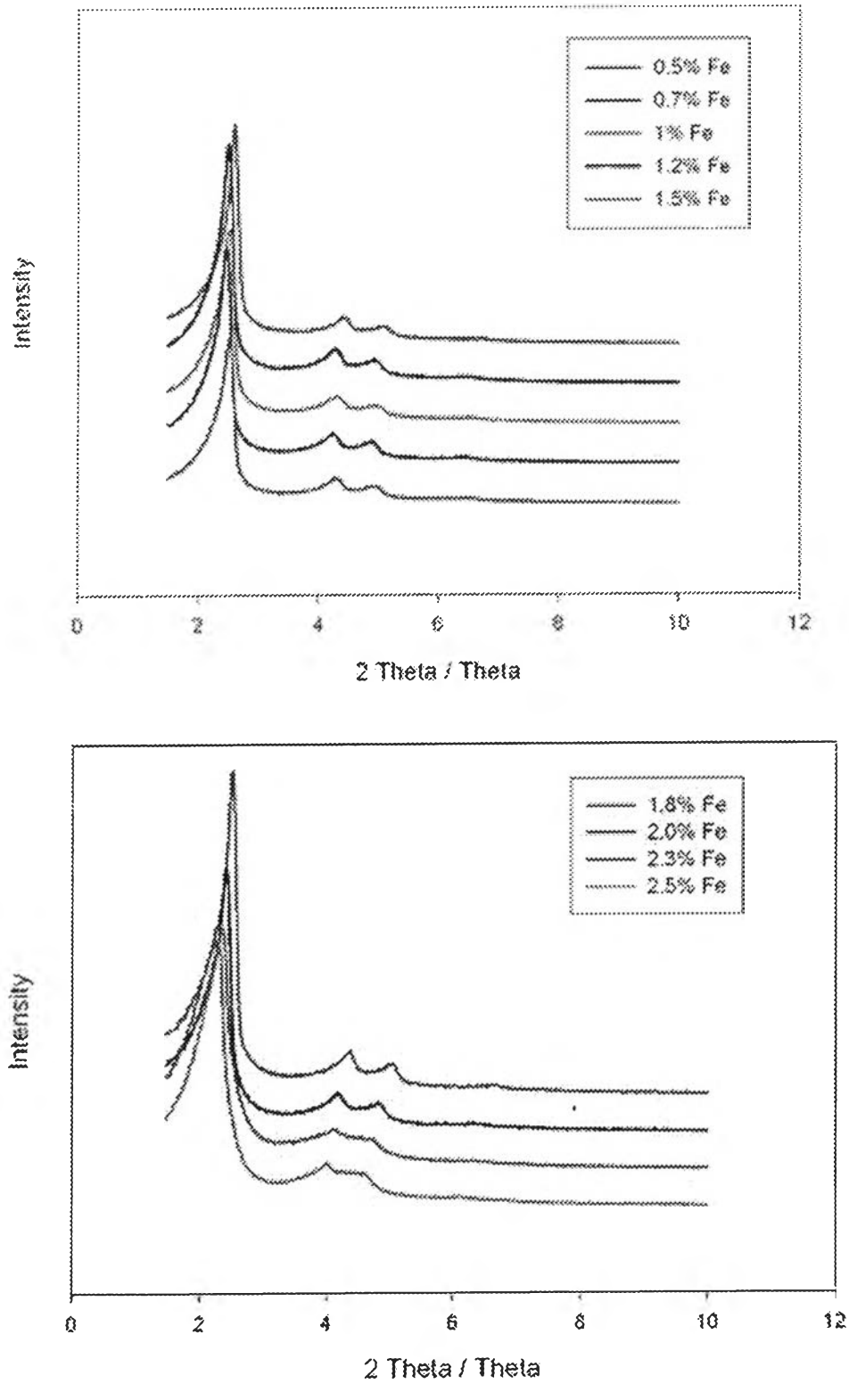

Figure 4.10 The XRD spectrum of synthesized MCM-41 at different amount of loaded Fe.

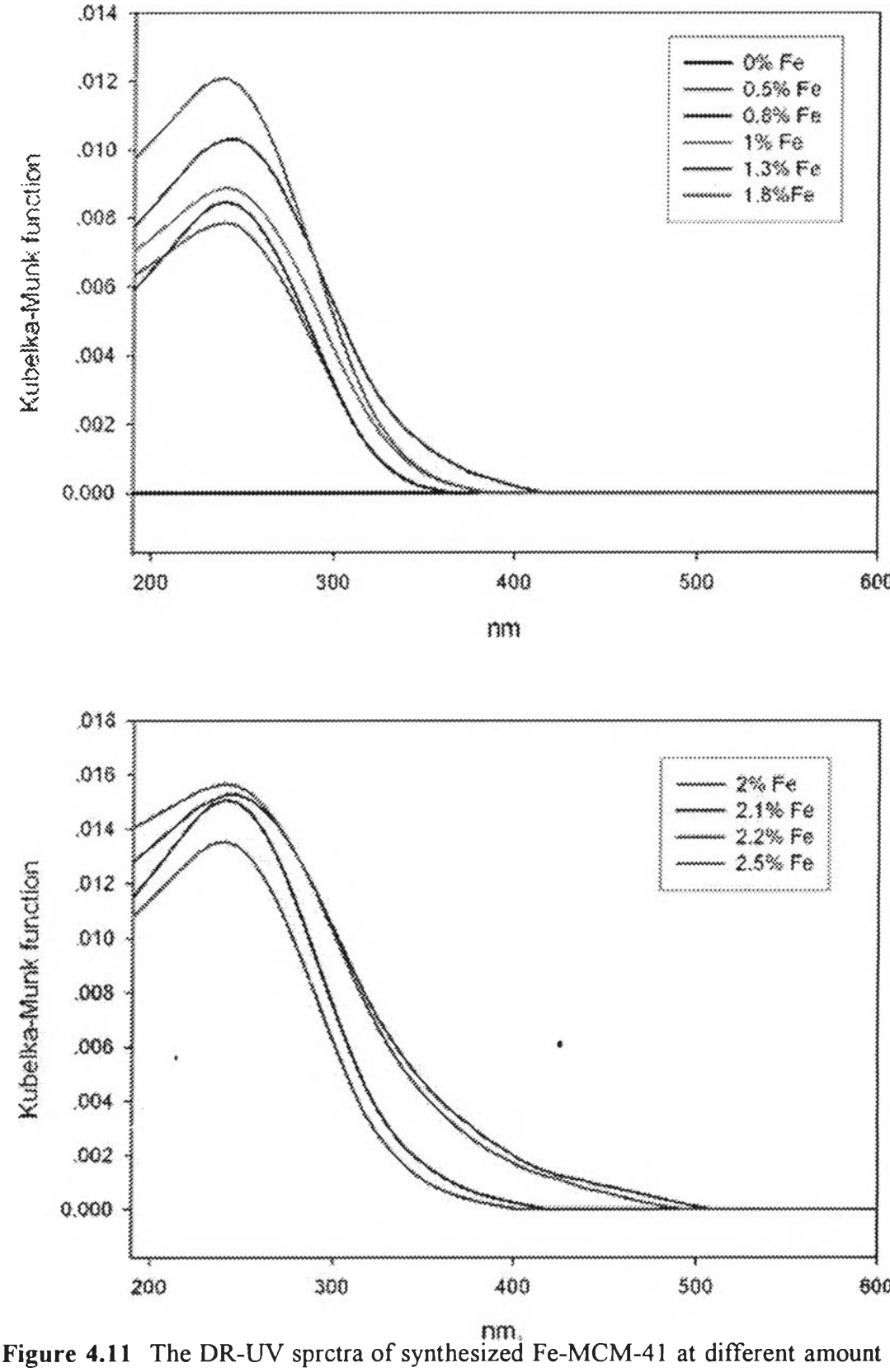

Figure 4.11 The DR-UV sprctra of synthesized Fe-MCM-41 at different amount of loaded Fe.

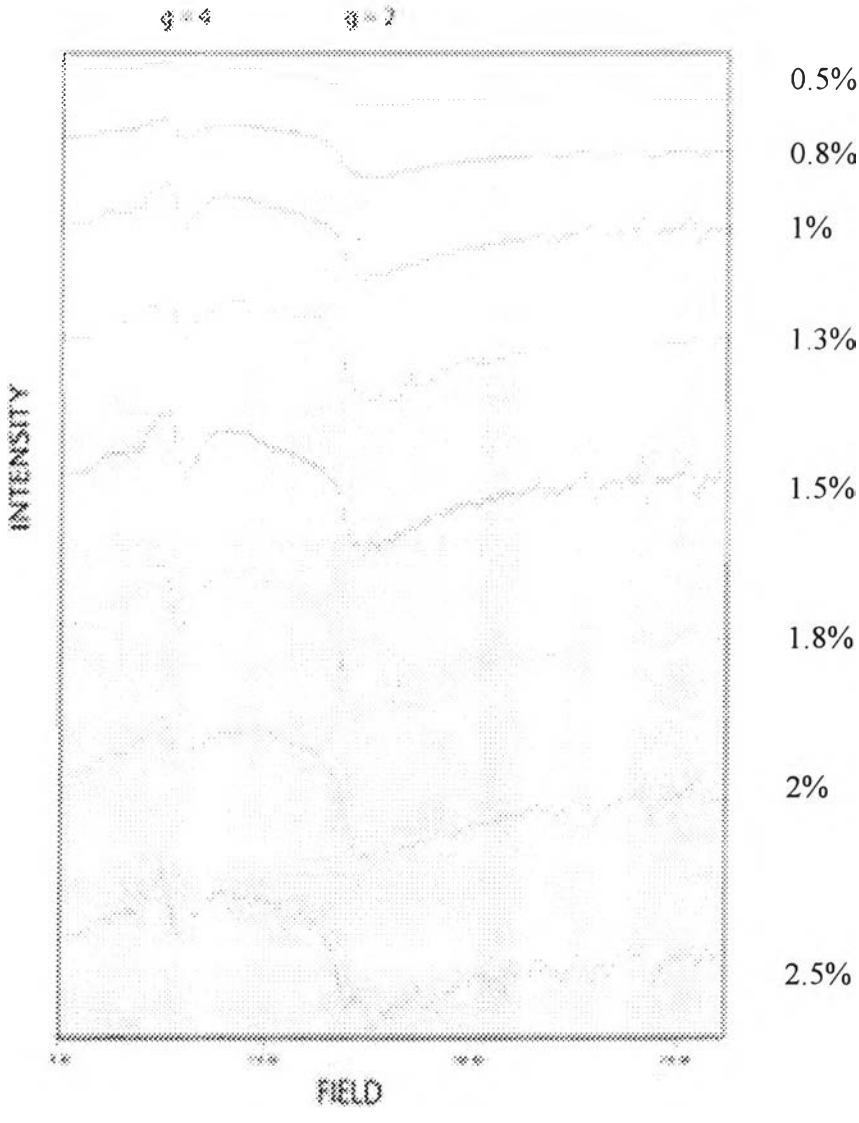

Figure 4.12 The ESR sprctra of synthesized Fe-MCM-41 at different amount of loaded Fe.

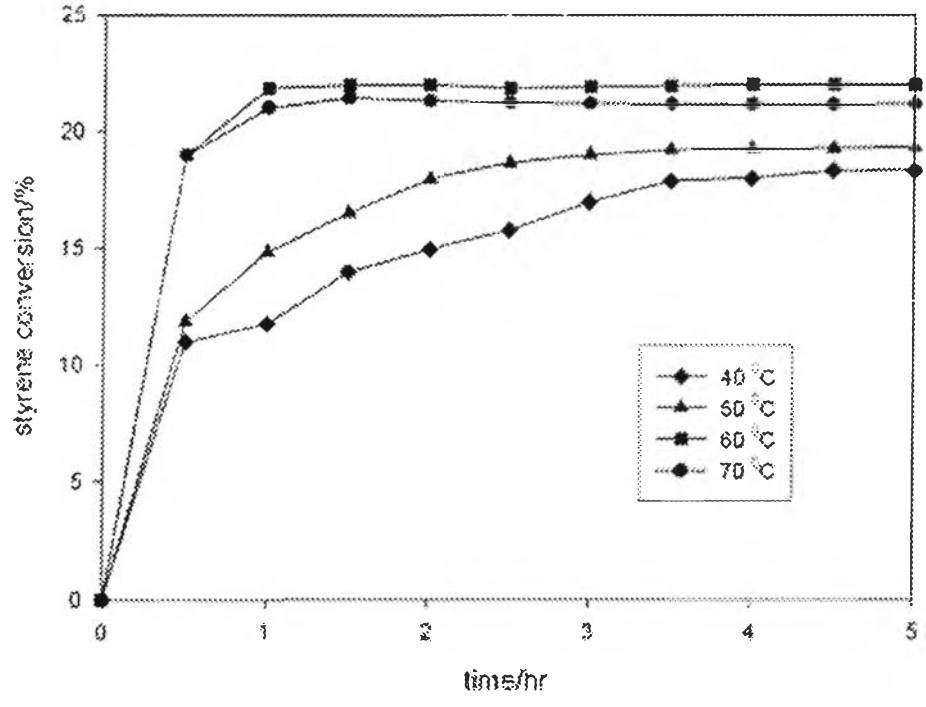

% Styrene conversion at various temperatures and reaction times.

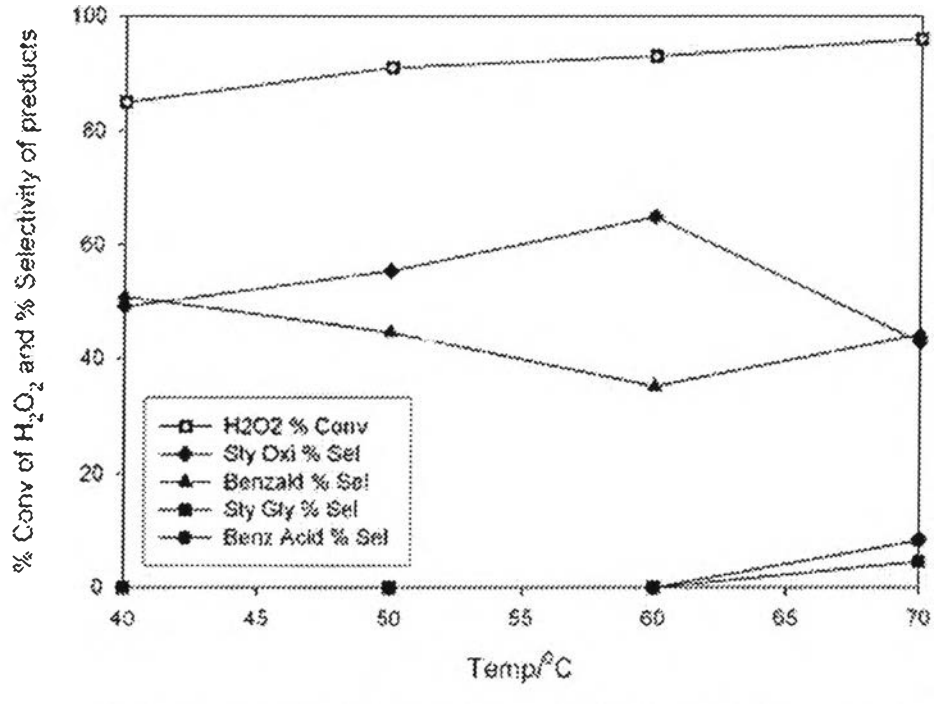

% Conversion of H_2O_2 and % selectivity of products at 2 hrs

Figure 4.13 Change of catalytic performance with temperature.

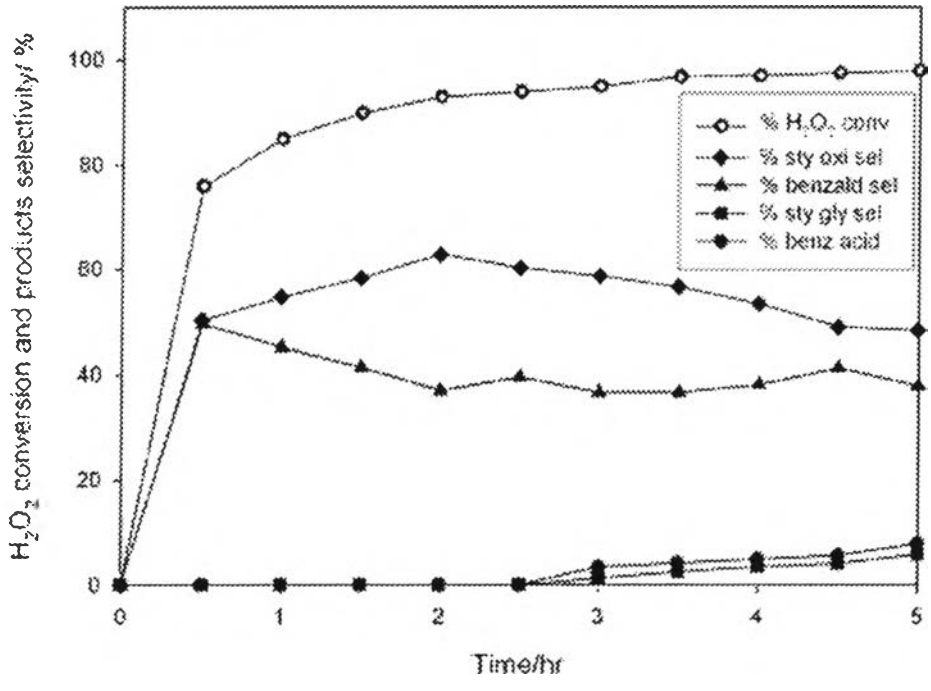

Figure 4.14 Change of catalytic performance with reaction time.

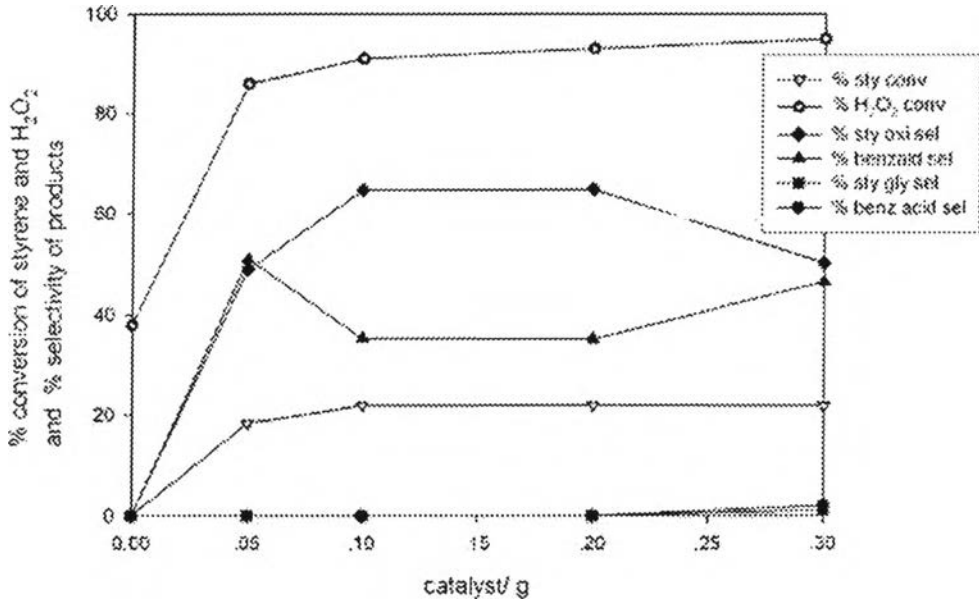

% Conversion of styrene and H_2O_2 and % selectivity of products

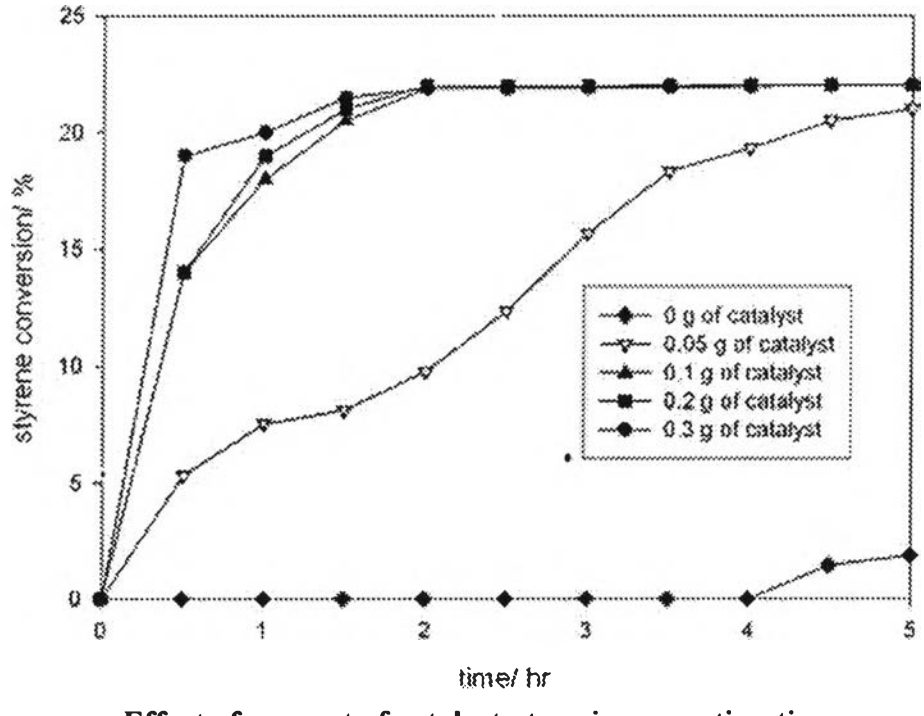

Effect of amount of catalyst at various reaction time

Figure 4.15 Change of catalytic performance with amount of catalyst.

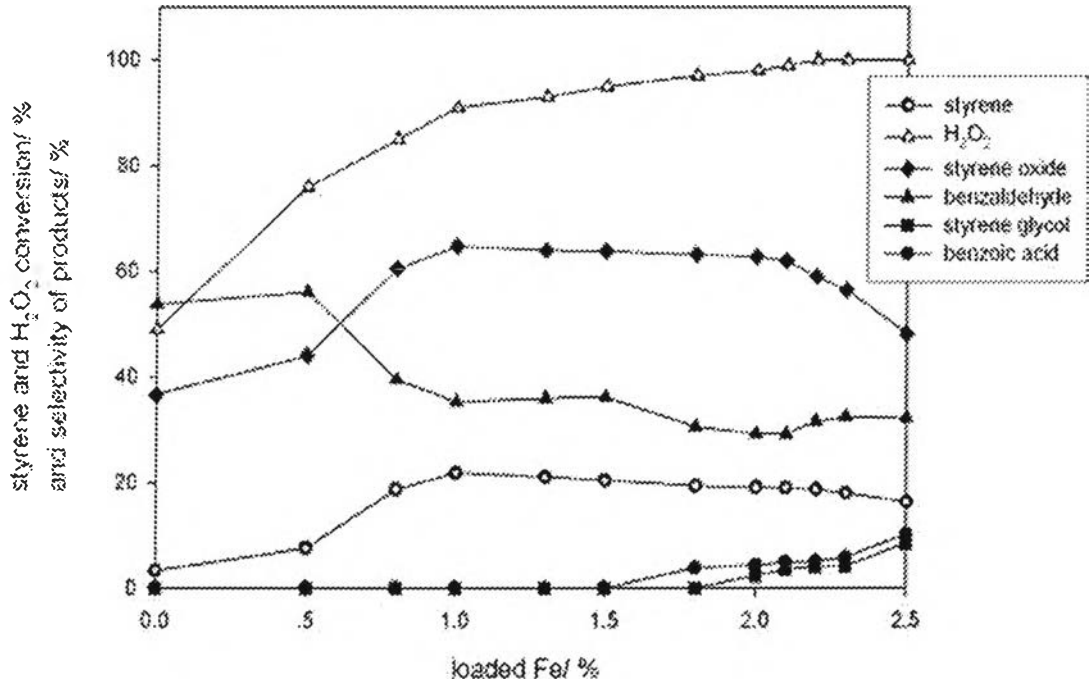

Figure 4.16 Change of catalytic performance with amount of loaded Fe.